

Delays in Spiking Neural Networks: A State Space Model Approach

Sanja Karilanova, Subhrakanti Dey, Ayça Özçelikkale

Department of Electrical Engineering, Uppsala University, Sweden

{Sanja.Karilanova, Subhrakanti.Dey, Ayca.Ozcelikkale}@angstrom.uu.se

I. ABSTRACT

Spiking neural networks (SNNs) are biologically inspired, event-driven models that are suitable for processing temporal data and offer energy-efficient computation when implemented on neuromorphic hardware. In SNNs, richer neuronal dynamics allows capturing more complex temporal dependencies, with delays playing a crucial role by allowing past inputs to directly influence present spiking behavior. We propose a general framework for incorporating delays into SNNs through additional state variables. The proposed mechanism enables each neuron to access a finite temporal input history. The framework is agnostic to neuron models and hence can be seamlessly integrated into standard spiking neuron models such as LIF and adLIF. We analyze how the duration of the delays and the learnable parameters associated with them affect the performance. We investigate the trade-offs in the network architecture due to additional state variables introduced by the delay mechanism. Experiments on the Spiking Heidelberg Digits (SHD) dataset show that the proposed mechanism matches the performance of existing delay-based SNNs while remaining computationally efficient. Moreover, the results illustrate that the incorporation of delays may substantially improve performance in smaller networks. Code available at <https://github.com/sannkka/Modeling-State-Delays-in-SNNs>.

Index Terms—spiking neural networks (SNN), state-space models (SSM), neuromorphic, delays, memory.

II. INTRODUCTION

Spiking Neural Networks (SNNs) [1] have emerged as a more biologically plausible class of neural models compared to conventional artificial neural networks (ANNs), offering promising advantages in temporal processing and energy efficiency, particularly when deployed on neuromorphic hardware [2]. SNNs encode information in the timing of discrete spikes, allowing them to capture temporal structure and making them well suited for modeling time-dependent signals such as audio [3], sensory [4], or visual patterns [5]. Despite these advantages, achieving performance comparable to that of ANNs remains an open challenge, in part due to the limited temporal expressivity of current SNN models.

S. Karilanova and A. Özçelikkale acknowledge the support of Center for Interdisciplinary Mathematics (CIM), and AI4Research, Uppsala University. The computations were enabled by resources provided by the National Academic Infrastructure for Supercomputing in Sweden (NAIIS), partially funded by the Swedish Research Council through grant agreement no. 2022-06725.

In biological neural systems, temporal delays play a critical computational role. Delays that enable neurons to integrate information from multiple past moments support tasks such as hearing [6] and brain activity [7]. Inspired by these findings, numerous works have explored incorporating delays into computational SNNs models. Theoretical analyses have shown that an SNN with k adjustable delays can compute a much richer class of functions than a threshold circuit with k adjustable weights [8]. Empirical studies have also demonstrated improved performance when optimizing spike transmission delays along with synaptic weights or membrane time constants [9], [10]. These results suggest that delays can enrich the information processing capabilities of SNNs and their internal representation. However, despite these promising results, practical methods for introducing structured, scalable, and differentiable forms of delay into modern deep SNNs remains an ongoing research problem.

In this work, we propose a method based on State Space Models (SSMs) for equipping SNNs with delays. The method uses a time-shift based state transition, which enables each neuron to access both its current input and the most recent history of past input values. The formulation is general and can be incorporated into arbitrary spiking neuron models. Conceptually, the framework bridges ideas from SSMs and SNNs, allowing SNNs to capture a fixed number of past inputs in a structured and interpretable manner.

Our contributions can be summarized as follows:

- We propose a method for incorporating delays within the state dynamics through additional delay variables, enabling neurons to access a finite temporal history of inputs.
- The proposed formulation is general and easily integrable into existing spiking neuron models, including LIF, adLIF, and RadLIF.
- We conduct a systematic analysis of delay order, i.e. the number of allowed past inputs, and their associated learnable parameters, and study the trade-offs between the number of neurons in the network and the delay order.
- The proposed framework introduces either no additional trainable parameters (i.e. when the delay parameters are not trained) or a number of trainable parameters comparable to the other SNN delay models.

The proposed models achieve performance comparable to existing delay-based SNN approaches on the Spiking Heidelberg Digits (SHD) dataset. Moreover, the observed trade-offs highlight promising directions for future exploration,

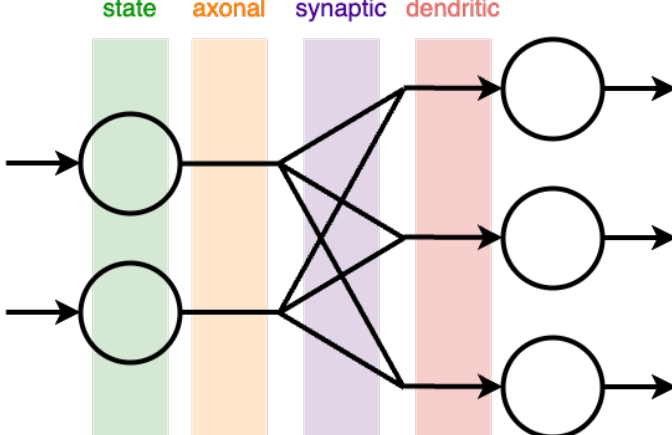


Fig. 1: Illustration of different approaches of modeling delays. Our proposed delays are modeled within the state dynamics of the neuron (green). Figure is inspired by [11, Fig. 3(a)].

particularly showing that incorporating delays can substantially improve accuracy in smaller SNNs where the neuron count limits temporal capacity.

III. RELATED WORK

In the SNN literature, three main types of delays are commonly modeled: axonal delays, applied to the output of a neuron [10], [12], [13]; dendritic delays, applied to its input [14]; and synaptic delays, specific to each connection between neuron pairs [9], [15]–[18]. In contrast to these formulations, we propose an SSM based approach where delays are modeled within the state dynamics of the neuron. See Figure 1 for a schematic illustration.

The most common ways to model delays in SNNs is to learn a single delay value applied to each spike [12], or to employ temporal convolutions [16]. Several works explore the role of delays in SNNs by jointly training weights and delays [9], learning only delays [15], or showing that heterogeneous delays can reduce weight-precision requirements [10]. Others relate delays to temporal parameters such as time constants [19] or study their role in the formation of temporal hierarchies between layers [20]. In these works, various learning algorithms have been used, such as variations of backpropagation through time (BPTT) [12], [16], [18], [21], biologically inspired spike-timing-dependent plasticity (STDP) [17], and exact spike-time gradients [11], [22]. Our formulation represents delays as state variables evolving over time. This structure remains compatible with BPTT, enabling training with the popular surrogate-gradient methods [23] used to train SNNs.

Delays have long been studied in fields such as signal processing and control theory. In discrete-time dynamical systems, they are typically modeled through delay-difference or state-space formulations, where past states are explicitly included to capture finite memory effects [24], [25]. Recently, modern deep SSMs, which stack multiple state-space layers combined with nonlinearities, have demonstrated strong performance in sequence modeling tasks [26], [27]. Even more recently, parameterization has been introduced in deep SSMs, effectively capturing delayed state dependencies [28], [29].

We build on this formulation to represent controllable delays within spiking neural network models. A common approach in modern SNNs embeds spiking dynamics within SSMs, where at each time step the output of the deep SSM layer is passed through a firing threshold function [30]–[34]. We continue in this direction by utilizing the SSM perspective on delay modeling to spiking neural architectures, enabling SNNs to incorporate structured temporal dependencies through the same principled state-space formulation.

IV. METHODS

A. Preliminaries

1) *General Spiking Neuron Model*: A single general feed-forward discrete-time n -state dimensional spiking neuron can be defined as [32], [33], [35]:

$$\mathbf{v}_s[t+1] = \mathbf{A}_s \mathbf{v}_s[t] + \mathbf{B}_s i_s[t] - \mathbf{R} s[t] \quad (1a)$$

$$s[t] = f_{\Theta}(\mathbf{v}_s[t]) = \begin{cases} 1 & \text{if } \mathbf{v}_s[t] \in \Theta \\ 0 & \text{otherwise} \end{cases} \quad (1b)$$

where $i_s[t] \in \mathbb{R}^{1 \times 1}$ is the input to the neuron, $s[t] \in \mathbb{R}^{1 \times 1}$ is the output of the neuron and $\mathbf{v}_s \in \mathbb{R}^{n_s \times 1}$ is the state variable of the neuron. The matrices $\mathbf{A}_s \in \mathbb{R}^{n_s \times n_s}$, $\mathbf{B}_s \in \mathbb{R}^{n_s \times 1}$, $\mathbf{R} \in \mathbb{R}^{n_s \times 1}$ represents the leak, impact of the input and the reset feedback, respectively. The spiking behavior is described by $f_{\Theta}(\cdot)$, where the neuron spikes when the state enters into the region described by Θ .

The neuron model in (1) generalizes several commonly used formulations, including the Leaky Integrate-and-Fire (LIF) and adaptive LIF (adLIF) neurons, see [32], [33], [35] for illustration of such representations.

Spiking neural networks are built by connecting neurons such that the output spikes from the previous (pre-synaptic, $l-1$) layer serve as inputs to the next (post-synaptic, l) layer. Let L_{pre} and L_{post} be the number of neurons in the pre and post synaptic layer. Let $\mathbf{W} \in \mathbb{R}^{L_{\text{post}} \times L_{\text{pre}}}$ be the weight matrix connecting the two layers, and $\mathbf{V} \in \mathbb{R}^{L_{\text{post}} \times L_{\text{post}}}$ be the weight matrix associated with the recurrent connections between neurons in a layer. Then $i[t] = \mathbf{W} \times s^{l-1}[t] + \mathbf{V} \times s^l[t]$, where $s^{l-1}[t]$ and $s^l[t]$ are a vector of all the spikes from the previous and current layer, respectively.

2) *State Space Model with Time Shift State Transition Matrix*: A discrete-time time-invariant linear SSM can be written as [36]:

$$\mathbf{v}_d[t+1] = \mathbf{A}_d \mathbf{v}_d[t] + \mathbf{B}_d i_d[t] \quad (2a)$$

$$\mathbf{y}_d[t] = \mathbf{C}_d \mathbf{v}_d[t] + \mathbf{D}_d i_d[t], \quad (2b)$$

where $\mathbf{v}_d[t], i_d[t], \mathbf{y}_d[t]$ denote the state vector, the input vector, and the output vector, respectively. Here, the state transition matrix $\mathbf{A}_d \in \mathbb{R}^{n_d \times n_d}$ describes the internal recurrent behavior of SSM. The matrices $\mathbf{B}_d \in \mathbb{R}^{n_d \times 1}$, $\mathbf{C}_d \in \mathbb{R}^{n_{\text{out}} \times n_d}$, $\mathbf{D}_d \in \mathbb{R}^{n_{\text{out}} \times 1}$ describe the interaction of the SSM through its inputs and outputs.

The lower shift matrix is a structured form of the state-transition matrix with nonzero elements only on the subdiago-

nal. Let \mathbf{A}_d be the lower shift matrix:

$$\mathbf{A}_d = \begin{bmatrix} 0 & 0 & \dots & 0 & 0 \\ a_1 & 0 & \dots & 0 & 0 \\ 0 & a_2 & \dots & 0 & 0 \\ \vdots & \ddots & \ddots & \vdots & \vdots \\ 0 & 0 & \dots & a_{n_d-1} & 0 \end{bmatrix} \text{ i.e., } \quad (3a)$$

$$[\mathbf{A}_d]_{i,j} = \begin{cases} a_j & \text{for } i-1 = j \\ 0 & \text{otherwise} \end{cases} \quad (3b)$$

where $[\mathbf{A}_d]_{i,j}$ represents the i th row j th column element of the matrix \mathbf{A}_d . Let

$$\mathbf{B}_d = [1, 0, \dots, 0]^T. \quad (4)$$

Then for the SSM state variable \mathbf{v}_d defined in (2) and initial state $\mathbf{v}_d[0] = \mathbf{0}^{n_d \times 1}$ we have:

$$\begin{aligned} \mathbf{v}_d[1] &= [i_d[1], 0, 0, \dots, 0]^T \\ \mathbf{v}_d[2] &= [i_d[2], a_1 i_d[1], 0, \dots, 0]^T \\ \mathbf{v}_d[3] &= [i_d[3], a_1 i_d[2], a_2 a_1 i_d[1], \dots, 0]^T \\ &\vdots \\ \mathbf{v}_d[t] &= [i_d[t], a_1 i_d[t-1], a_2 a_1 i_d[t-2], \dots, \\ &\quad (\prod_{k=1}^{n-1} a_k) i_d[t-n_d+1]]^T. \end{aligned}$$

Hence, at time t the state variable \mathbf{v}_d is a vector with entries equal to the last n inputs to the system parametrized by the parameters a_i , where n is the state dimension.

Note that although the a_i parameters are free in general, in this paper we set $a_i = 1$ for all i . Under this choice, the delay component \mathbf{v}_d reduces to a simple temporal memory of the input, i.e.,

$$\mathbf{v}_d[t] = [i_d[t], i_d[t-1], i_d[t-2], \dots, i_d[t-n_d+1]]^T. \quad (5)$$

B. Proposed Model

Let \mathbf{v}_s be the state variable of the general spiking neuron in (1) with parameter matrices $\mathbf{A}_s, \mathbf{B}_s, \mathbf{C}_s$ and state dimension n_s . Let \mathbf{v}_d be the state variable of the time-shift SSM in Section IV-A2 with parameter matrices $\mathbf{A}_d, \mathbf{B}_d, \mathbf{C}_d$ and state dimension n_d . Our proposed spiking neuron model with state-delays is defined as:

$$\mathbf{v}_d[t+1] = \mathbf{A}_d \mathbf{v}_d[t] + \mathbf{B}_d i_d[t] \quad (6a)$$

$$\mathbf{v}_s[t+1] = \mathbf{A}_s \mathbf{v}_s[t] + \mathbf{B}_s i_s[t] + \mathbf{A}_{sd} \mathbf{v}_d[t] - \mathbf{R} s[t] \quad (6b)$$

$$\begin{aligned} s[t] &= f_{\Theta}(\mathbf{C}_s \mathbf{v}_s[t] + \mathbf{C}_d \mathbf{v}_d[t]) \\ &= \begin{cases} 1 & \text{if } (\mathbf{C}_s \mathbf{v}_s[t] + \mathbf{C}_d \mathbf{v}_d[t]) \in \Theta \\ 0 & \text{otherwise} \end{cases} \end{aligned} \quad (6c)$$

Here, $\mathbf{A}_{sd} \in \mathbb{R}^{n_s \times n_d}$ gives the parameters that delayed inputs in the state \mathbf{v}_d are multiplied with before they are added to the neuron state \mathbf{v}_s .

The above equations present a spiking neuron with additional access to temporal memory through the state variable $\mathbf{v}_d[t]$. The state dimension n_d defines the maximum order of the delays provided to the spiking neuron i.e. the number of directly accessible past quantities. The input i_s to \mathbf{v}_s , as defined in Section IV-A1, represents the input spikes to the neuron. The

TABLE I: Table of notation.

| Notation | Meaning |
|--|--|
| $\mathbf{v}_s[t]$ | State of the neuron's intrinsic components |
| $\mathbf{v}_d[t]$ | State of the neuron's delay component |
| n_s | Dimension of \mathbf{v}_s |
| n_d | Dimension of \mathbf{v}_d (delay order) |
| $\mathbf{A}_s, \mathbf{B}_s, \mathbf{C}_s$ | Linear model parameters of \mathbf{v}_s |
| $\mathbf{A}_d, \mathbf{B}_d, \mathbf{C}_d$ | Linear model parameters of \mathbf{v}_d |
| \mathbf{R} | Reset parameters |
| \mathbf{A}_{sd} | Delay parameters |
| $i_s[t]$ | Input to \mathbf{v}_s |
| $i_d[t]$ | Input to \mathbf{v}_d |
| $s[t]$ | Spike output of the neuron |
| l | Number of hidden layers |
| h | Number of neurons in a hidden layer |

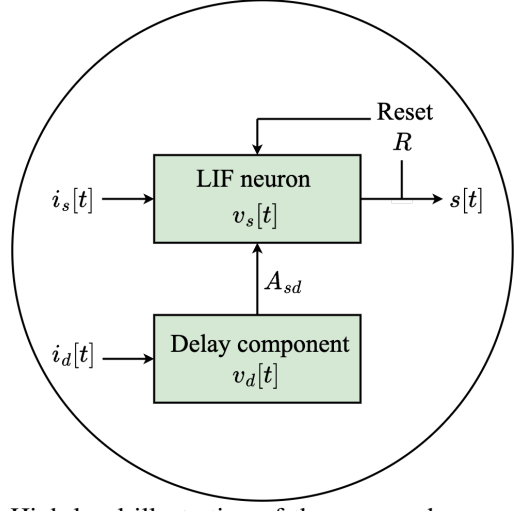


Fig. 2: High-level illustration of the proposed neuron model. The figure shows how the delay components are incorporated into the traditional SNN neuron model (LIF neuron shown).

input i_d to \mathbf{v}_d represents the input stored in the temporal memory. See Table I for an overview of the notation. Examples of the proposed models with LIF and adLIF neuron models are provided in Sections IV-B1 and IV-B2, respectively. A high-level visualization of the proposed model is presented in Figure 2.

1) *LIF and RLIF example*: The discrete-time Leaky Integrate-and-Fire (LIF) neuron, as defined in [3], with the additional proposed delays is given by:

$$\mathbf{v}_d[t+1] = \mathbf{A}_d \mathbf{v}_d[t] + \mathbf{B}_d i_d[t] \quad (7a)$$

$$u[t+1] = \alpha u[t] + (1 - \alpha) i_s[t] - \alpha \theta s[t] + \mathbf{A}_{sd} \mathbf{v}_d[t] \quad (7b)$$

$$s[t] = f_{\theta}(u[t]) = \begin{cases} 1 & \text{if } u[t] \geq \theta \\ 0 & \text{otherwise} \end{cases} \quad (7c)$$

where $i_s[t] = \mathbf{W} \times \mathbf{s}^{l-1}[t] + \mathbf{V} \times \mathbf{s}^l[t]$ for RLIF and $i_s[t] = \mathbf{W} \times \mathbf{s}^{l-1}[t]$ for LIF. For both RLIF and LIF, we have $i_d[t] = \mathbf{W} \times \mathbf{s}^{l-1}[t]$.

2) *adLIF and RadLIF example*: The Adaptive Leaky Integrate-and-Fire (adLIF) neuron is an extension of the LIF neuron with an additional recovery state variable, $w[t]$ [3]. Discrete-time adLIF neuron with the additional proposed delays

is:

$$\mathbf{v}_d[t+1] = \mathbf{A}_d \mathbf{v}_d[t] + \mathbf{B}_d i_d[t] \quad (8a)$$

$$\begin{aligned} u[t+1] &= \alpha u[t] + (1 - \alpha)[i_s[t] - w[t]] - \alpha \theta s[t] \\ &+ \mathbf{A}_{sd} \mathbf{v}_d[t+1] \end{aligned} \quad (8b)$$

$$w[t+1] = \alpha u[t] + \beta w[t] + b s[t] \quad (8c)$$

$$s[t] = f_\theta(u[t]) = \begin{cases} 1 & \text{if } u[t] \geq \theta \\ 0 & \text{otherwise.} \end{cases} \quad (8d)$$

The inputs $i_s[t]$ and $i_d[t]$ are as defined for RLIF in Section IV-B1 with a correspondence between LIF and adLIF, and RLIF and RadLIF.

C. Delay parameters

We now provide an overview of all parameters related to the additional delay variable \mathbf{v}_d in (6). We have \mathbf{A}_d given by (3) under $a_i = 1$ and \mathbf{B}_d given by (4), hence they are fixed and non-trainable. Under LIF/RLIF neuron models of (7) and adLIF/RadLIF neuron models of (8), we do not use \mathbf{C}_d . Hence, the only additional (possibly trainable) parameter is \mathbf{A}_{sd} . In the rest of this section, we focus on \mathbf{A}_{sd} .

The matrix of parameters \mathbf{A}_{sd} plays a central role in our development, as it determines the contribution of the delay variable \mathbf{v}_d when added to the intrinsic neuron state \mathbf{v}_s , see (6). We consider four different settings for the elements of \mathbf{A}_{sd} :

- 1) $\mathbf{A}_{sd} = \text{Ones}$, where $[\mathbf{A}_{sd}]_{ij} = 1$
- 2) $\mathbf{A}_{sd} = \text{Linear decay}$, where $[\mathbf{A}_{sd}]_{ij} = (n_d - j) \frac{1}{n_d}$
- 3) $\mathbf{A}_{sd} = \text{Exponential decay}$, where $[\mathbf{A}_{sd}]_{ij} = e^{-0.5j}$
- 4) $\mathbf{A}_{sd} \sim \text{Uniform distribution}$, where $[\mathbf{A}_{sd}]_{ij} \sim U(0, 1)$

The equal sign $=$ is used in the cases where the elements of \mathbf{A}_{sd} are deterministic, while the sign \sim is used in the case where the elements of \mathbf{A}_{sd} are random. The matrix of delay parameters \mathbf{A}_{sd} can be trainable or fixed. When it is fixed, its elements do not change during the training of the SNN and remain as initially set. When it is trainable, the initial set values of \mathbf{A}_{sd} represent their initialization, and they change during the training phase without the constraint of preserving the distribution their initialization had, i.e., for instance if $[\mathbf{A}_{sd}]_{ij}$ is initialized as 'Ones', the parameters do not stay all ones or all equal. In Section VI we distinguish these cases by stating whether \mathbf{A}_{sd} is non-trainable or trainable.

We now illustrate how the matrix \mathbf{A}_{sd} determines the contribution of the delayed component $\mathbf{v}_d[t]$ in (5). The contributing delay component $\mathbf{A}_{sd} \mathbf{v}_d[t]$ is simply a weighted average of the past n_d inputs $i_d[t]$. In particular, we have the following cases:

- 1) For $\mathbf{A}_{sd} = \text{Ones}$:

$$\mathbf{A}_{sd} \mathbf{v}_d[t] = i_d[t] + i_d[t-1] + i_d[t-2] + \dots$$

- 2) For $\mathbf{A}_{sd} = \text{Linear Decay}$: For instance, with $n_d = 5$:

$$\mathbf{A}_{sd} \mathbf{v}_d[t] = i_d[t] + 0.8i_d[t-1] + 0.6i_d[t-2] + \dots$$

- 3) For $\mathbf{A}_{sd} = \text{Exponential Decay}$: For instance, with $n_d = 5$:

$$\mathbf{A}_{sd} \mathbf{v}_d[t] = i_d[t] + 0.60i_d[t-1] + 0.34i_d[t-2] + \dots$$

- 4) For $\mathbf{A}_{sd} \sim \text{Uniform}$. Here, the elements are random. A particular realization could be:

$$\mathbf{A}_{sd} \mathbf{v}_d[t] = 0.1i_d[t] + 0.9i_d[t-1] + 0.2i_d[t-2] + \dots$$

D. Computational complexity

The proposed neuron model with delays, given in (6), extends the baseline formulation in (1) by introducing an additional state variable \mathbf{v}_d and its associated parameters \mathbf{A}_d , \mathbf{B}_d , \mathbf{A}_{sd} , and \mathbf{C}_d . The dimensionality of these matrices is determined by the delay order n_d . In this section, we analyze how this additional state and its parameters influence the computational complexity of the spiking neuron for the case of LIF and adLIF neuron as defined in Section IV-B1 and IV-B2.

1) *Number of trainable parameters*: The baseline definition of the LIF neuron model has 1 trainable parameter, i.e., α , while the adLIF neuron model has 4 trainable parameters, i.e., α, β, a, b . Let l be the number of hidden layers, each with h number of neurons. Let c_{in} and c_{out} be the number of input and output channels to the network. Then, the number of trainable parameters introduced by individual components of the networks is given by:

- feedforward synaptic connections: $c_{in}h + h^2(l-1) + hc_{out}$
- recurrent synaptic connections: $l(h^2 - h)$
- neuron parameters: lh for LIF and $= 4lh$ for adLIF
- normalization layers: $2(hl + c_{out})$
- delays: n_dhl if \mathbf{A}_{sd} trainable, 0 otherwise.

From the above calculations, we observe that the number of additional parameters introduced by the delay mechanism is n_dhl , and only if the matrix \mathbf{A}_{sd} is trainable. Even in this case, the number of delay-related parameters remains relatively small compared to the number of synaptic connections, which scale as h^2 . Relatively small values of n_d get competitive performance, see Section VI. Hence, since h is much larger than both n_d or l in both LIF and adLIF networks, the added computational and parametric overhead of incorporating delays is negligible.

In the remainder of this section, we compare the number of trainable parameters introduced by our proposed delay modeling with those reported in related work.

In [9, Table 1], the inclusion of delays increased the total number of parameters from 38.7k to 75.8k i.e., by 37.1k parameters. For the same network architecture we increase the total number of parameters by $n_dhl = n_d \times 128 \times 2$ parameters. For $n_d = 10$, this corresponds to approximately 2.6k parameters, which is an order of magnitude smaller than in [9].

[10, Section 2.1] reports that each neuron maintains a single learned delay shared across all outgoing connections, resulting in $\mathcal{O}(h)$ parameter scaling. In our formulation, up to n_d delay-related parameters can be trained per neuron, where the overall scaling remains $\mathcal{O}(h)$. As noted in [10], this is considerably more efficient than the $\mathcal{O}(h^2)$ scaling of synaptic weights.

2) *Memory*: The state variable $\mathbf{v}_d \in \mathbb{R}^{n_d \times 1}$ can be seen as a memory buffer that stores n_d values per neuron.

The intrinsic neuron state $\mathbf{v}_s \in \mathbb{R}^{n_s \times 1}$ already contains n_s internal variables that evolve over time. For example, the standard LIF neuron has a single state variable, the membrane potential, resulting in $n_s = 1$. The adLIF, compared to the LIF, includes an additional threshold-adaptation variable, resulting in $n_s = 2$. When the delay variable \mathbf{v}_d is appended to the

TABLE II: Accuracy and number of parameters reported for delay-based SNN papers on the SHD dataset. M denotes millions of parameters.

| Paper | Accuracy | # params. |
|--|------------------------------------|---------------------|
| Learning DCLS [16] | 95.07 \pm 0.24 % | 0.2M |
| Co-learning [9] | 95.02 % | 0.076M |
| Learnable axonal delay [13] | 93.55 % | 0.21M |
| Event-based Delay [22] | 93.24 \pm 1.00 % | 0.5M ^(a) |
| Temporal Hierarchy [20] | 92.1 % ^(b) | - |
| Heterogeneous Delays [10] | 90.98 % | 0.1M ^(c) |
| Our (adLIF, $n_d = 5$, non-train. A_{sd}) | 94.1 \pm 0.5 % | 0.04M |

^(a) Read from [22, Fig. 5]

^(b) Read from [20, Fig. 5]

^(c) Read from [Fig.1c] [10]

intrinsic state v_s in (6), the number of state variables for each neuron increases from n_s to $n_s + n_d$.

At the network level, this increase applies to all hidden layers l with h neurons, increasing the total number of stored state variables from $n_s h l$ to $(n_s + n_d) h l$. However, as noted in Section IV-D1, the values n_s, n_d and l are all much smaller than h . Consequently, in both cases, with or without delays, the memory footprint scales predominantly with h .

V. EXPERIMENTAL SET-UP

1) *Network Architecture and Training*: In all experiments, a network with two hidden layers is used with batch normalization layers [37] and an accumulative output layer with cross entropy loss. Each model is trained using BPTT with surrogate gradient [23], AdamW optimizer [38] and cosine learning rate scheduler. We present further details for training and network parameters in Section IX-A.

2) *Dataset*: The Spiking Heidelberg Digits (SHD) dataset was introduced to standardize the evaluation of neuromorphic learning models [39]. It consists of spike sequences derived from microphone recordings using the Lauscher artificial cochlea model. The dataset contains 20 classes of spoken digits 0 to 9 in both German and English. It has 8156 training and 2264 test samples. Each sample is represented by 700 input channels. This dataset is primarily used for classification tasks, where the goal is to identify the spoken digit from the input spike sequence. Further details on dataset preprocessing and usage are provided in Section IX-B.

VI. RESULTS

In this section, we discuss the numerical experiments presented in Tables II, III, IV, V. Specifically in Section VI-A we comment on the performance of our proposed method in comparison to the works in the literature. In Sections VI-B, VI-C, VI-D, and VI-E we comment on the varying order of delays, the delay parameters, the corresponding network training time, and the varying number of neurons used, respectively. In the final Section VI-F we discuss the effect of trainable and non-trainable delay parameters.

A. Comparison to literature

In this section, we compare our best performance presented in this paper with the performances of SHD dataset with other SNN works which include delays, see Table II. We observe

that our model is comparable both in terms of performance and in terms of number of parameters used.

Note that in general, the highest average accuracy reported over multiple initialization instances for the SHD dataset using SNNs is 95.07% [16], which is included in Table II. The benchmark performance using a non-spiking encoding of the same data and a recurrent neural network is 99.69% [40].

B. Order of delays

In this section, we discuss the varying order of delays i.e., we compare $n_d = 0, 5$ and 10 , see Table III.

We observe that increasing the delay order from $n_d = 0$ (i.e. no delay, hence the same as the traditional neuron types) to $n_d = 5$ or $n_d = 10$ in the LIF, adLIF, and RadLIF neurons either maintains (i.e. the performance with and without delay are within standard deviations of each other) or improves performance. For instance, in Table IIIa for the adLIF neuron model, the baseline accuracy with $n_d = 0$ is $92.0 \pm 0.4\%$, while for $A_{sd} = \text{Uniform}$ and $n_d = 5$ the accuracy rises to $94.1 \pm 0.5\%$, indicating an improvement beyond the standard deviation range. In contrast, the RLIF neuron either maintains its performance or shows only a slight decrease when delays are introduced. For example, in Table IIIa for the RLIF neuron model, the baseline accuracy with $n_d = 0$ is $90.6 \pm 0.5\%$, while for $A_{sd} = \text{Ones}$ and $n_d = 5$ the accuracy drops to $87.7 \pm 1.1\%$, indicating a performance drop beyond the standard deviation range.

When comparing $n_d = 5$ and $n_d = 10$, the results remain within the standard deviation of each other, suggesting that increasing the delay order to $n_d = 10$ does not yield additional benefits beyond what $n_d = 5$ already captures.

C. Delay parameters

In this section we investigate the impact of using various delay parameter settings for A_{sd} . In particular, we explore $A_{sd} = \text{Ones}$, Linear Decay, Exponential Decay, and $A_{sd} \sim \text{Uniform}$, see Section IV-C for more details of the setting. Table III provides the associated results.

We do not observe a consistent trend that holds in all values of n_d and in all neuron types. Most of the accuracy values are within the standard deviation of each other. The remaining differences appear to be model-specific. For instance, considering the average performance of the adLIF neuron, the best configuration for a non-trainable A_{sd} is the Uniform setting, whereas for a trainable A_{sd} , the Exponential Decay initialization yields the highest accuracy.

D. Training time

In this section, we discuss the additional training time introduced by using delays, see Table IV. We first focus on the increase in training time when using $n_d = 5$ compared to the baseline with no delay. The smallest ratio increase, $\frac{13.1}{8.6} = 1.5$, occurs for the adLIF model with a non-trainable A_{sd} , while the largest, $\frac{12.5}{6.5} = 1.8$, is observed for the LIF model with a trainable A_{sd} . Increasing n_d from 5 to 10 results in only a negligible change in training time.

TABLE III: Test accuracy on the SHD dataset across combinations of neuron model, delay parameters \mathbf{A}_{sd} , and delay order n_d . All networks consist of two hidden layers with $h = 128$ neurons each. Bold values indicate the best performance for each neuron model (per row).

| (a) \mathbf{A}_{sd} is non-trainable. | | | | | | | | | |
|---|------------------------------------|---------------------------------|------------------|---------------------------------------|------------------|---------------------------------------|------------------|---------------------------------------|------------------|
| Neuron Model | No delay | $\mathbf{A}_{sd} = \text{Ones}$ | | $\mathbf{A}_{sd} = \text{Lin. Decay}$ | | $\mathbf{A}_{sd} = \text{Exp. Decay}$ | | $\mathbf{A}_{sd} \sim \text{Uniform}$ | |
| | | $n_d = 5$ | $n_d = 10$ | $n_d = 5$ | $n_d = 10$ | $n_d = 5$ | $n_d = 10$ | $n_d = 5$ | $n_d = 10$ |
| LIF | $85.9 \pm 1.2\%$ | $86.6 \pm 1.2\%$ | $83.8 \pm 2.0\%$ | $86.6 \pm 0.8\%$ | $85.9 \pm 0.8\%$ | $86.7 \pm 0.7\%$ | $86.0 \pm 0.9\%$ | $87.2 \pm 1.6\%$ | $86.7 \pm 0.8\%$ |
| RLIF | $90.6 \pm 0.5\%$ | $87.7 \pm 1.1\%$ | $87.1 \pm 1.1\%$ | $88.8 \pm 1.0\%$ | $87.8 \pm 0.6\%$ | $87.9 \pm 1.7\%$ | $89.0 \pm 0.7\%$ | $89.6 \pm 1.0\%$ | $88.0 \pm 0.9\%$ |
| adLIF | $92.0 \pm 0.4\%$ | $92.1 \pm 0.2\%$ | $91.6 \pm 0.4\%$ | $93.3 \pm 0.9\%$ | $91.8 \pm 0.8\%$ | $93.3 \pm 0.4\%$ | $93.0 \pm 0.9\%$ | $94.1 \pm 0.5\%$ | $92.1 \pm 1.3\%$ |
| RadLIF | $93.4 \pm 1.1\%$ | $91.6 \pm 2.6\%$ | $91.2 \pm 2.2\%$ | $92.8 \pm 0.7\%$ | $92.4 \pm 0.9\%$ | $93.8 \pm 0.6\%$ | $93.5 \pm 0.4\%$ | $93.1 \pm 1.2\%$ | $92.1 \pm 1.2\%$ |

| (b) \mathbf{A}_{sd} is trainable. | | | | | | | | | |
|-------------------------------------|---------------------------------------|------------------|---|------------------|---|------------------------------------|---|------------------------------------|--|
| Neuron Model | $\mathbf{A}_{sd} = \text{Ones init.}$ | | $\mathbf{A}_{sd} = \text{Lin. Decay init.}$ | | $\mathbf{A}_{sd} = \text{Exp. Decay init.}$ | | $\mathbf{A}_{sd} \sim \text{Uniform init.}$ | | |
| | $n_d = 5$ | $n_d = 10$ | $n_d = 5$ | $n_d = 10$ | $n_d = 5$ | $n_d = 10$ | $n_d = 5$ | $n_d = 10$ | |
| LIF | $87.7 \pm 0.9\%$ | $88.2 \pm 1.0\%$ | $88.4 \pm 1.2\%$ | $89.1 \pm 0.3\%$ | $89.1 \pm 0.8\%$ | $89.6 \pm 1.1\%$ | $88.4 \pm 1.5\%$ | $89.5 \pm 0.5\%$ | |
| RLIF | $88.5 \pm 1.7\%$ | $87.9 \pm 1.3\%$ | $89.0 \pm 0.5\%$ | $89.5 \pm 1.2\%$ | $89.1 \pm 0.6\%$ | $90.3 \pm 0.9\%$ | $88.9 \pm 0.5\%$ | $89.7 \pm 0.8\%$ | |
| adLIF | $92.7 \pm 0.7\%$ | $91.9 \pm 0.5\%$ | $93.1 \pm 0.4\%$ | $92.7 \pm 0.5\%$ | $93.6 \pm 0.2\%$ | $93.6 \pm 1.1\%$ | $93.3 \pm 0.6\%$ | $92.6 \pm 0.5\%$ | |
| RadLIF | $93.4 \pm 0.8\%$ | $92.4 \pm 1.3\%$ | $94.0 \pm 0.2\%$ | $93.3 \pm 0.6\%$ | $93.4 \pm 0.5\%$ | $93.7 \pm 0.6\%$ | $93.7 \pm 0.6\%$ | $92.3 \pm 1.0\%$ | |

TABLE IV: Training time in minutes as average over the various delay parameters \mathbf{A}_{sd} settings for fixed n_d from Table III.

| (a) \mathbf{A}_{sd} non-trainable | | | |
|-------------------------------------|--------------------|---------------------|---------------------|
| Neuron Model | No delay | $n_d = 5$ | $n_d = 10$ |
| LIF | 6.5 ± 0.1 min. | 11.7 ± 0.1 min. | 12.0 ± 0.2 min. |
| RLIF | 7.9 ± 0.1 min. | 13.1 ± 0.2 min. | 12.9 ± 0.1 min. |
| adLIF | 8.6 ± 0.1 min. | 13.1 ± 0.3 min. | 13.4 ± 0.6 min. |
| RadLIF | 9.6 ± 0.1 min. | 15.4 ± 0.2 min. | 15.1 ± 0.1 min. |

| (b) \mathbf{A}_{sd} trainable | | | |
|---------------------------------|---------------------|---------------------|--|
| Neuron Model | $n_d = 5$ | $n_d = 10$ | |
| LIF | 12.5 ± 0.2 min. | 12.7 ± 0.3 min. | |
| RLIF | 13.9 ± 0.2 min. | 13.7 ± 0.1 min. | |
| adLIF | 14.1 ± 0.2 min. | 13.9 ± 0.1 min. | |
| RadLIF | 15.9 ± 0.4 min. | 16.0 ± 0.3 min. | |

E. Number of neurons vs order of delays

In this section, we discuss the combined effect of the number of neurons in the hidden layers h and the order of delays n_d , see Table V.

The impact of increasing n_d on the performance depends on the number of neurons h . For $h \geq 32$, using delays ($n_d = 10, 50$ or 100) maintains performance at a level similar to no-delay or slightly reduces it. In contrast, for smaller networks with $h \leq 16$, using delays yields a clear improvement over the baseline no-delay performance.

It is worth noting that, in our implementation, the input sequences of the SHD dataset have a length of 100. Consequently, setting $n_d = 100$ allows the network to access the entire temporal history of each sample at every time step.

F. Trainable vs non-trainable delay parameters

In this section, we compare the results obtained with trainable and non-trainable \mathbf{A}_{sd} matrices.

Comparing Tables IIIa and IIIb, we observe that the results are generally within the standard deviation of each other, except for the LIF case, where the trainable \mathbf{A}_{sd} provides a clear performance benefit. Similarly, Tables Va and Vb show no meaningful performance difference between the two configurations.

Tables IVa and IVb indicate that the additional training time required when \mathbf{A}_{sd} is trainable is negligible < 1 minute, which

further supports the discussion in Section IV-D1 regarding the small computational complexity overhead when using our proposed delays.

VII. DISCUSSIONS

The results suggest that the LIF and adLIF neurons may not be fully capable of exploiting the introduced delay mechanism. Their limited state dimensionality and small number of free parameters likely restrict the model's ability to fully utilize temporal depth introduced by the delay mechanism. More complex neuron models with richer internal dynamics might benefit more from the proposed delay formulation.

We did not perform any dedicated hyperparameter optimization (HPO) in this study. Conducting a thorough HPO for each neuron type and delay configuration could further improve performance and potentially alter observations.

From a neuromorphic computing perspective, an important open question is which of the proposed delay neuron models can be implemented efficiently on hardware. Implementing delays on hardware has been explored [11], [41]–[43], programmable delays can be implemented on various hardware including Intel Loihi [44], IBM TrueNorth [45], SpiNNaker [46], and SENeCA [47]. Whether similar implementations can be performed for the proposed models is an open question.

VIII. CONCLUSION

In this work, we proposed a general framework for modeling delays within spiking neuron dynamics by introducing additional state variables that encodes delayed information. This formulation enables neurons to access a finite temporal history. The framework is general and can be easily integrated into various spiking neuron models.

We analyzed different aspects of this formulation, including the order of delays, delay parameters and their optimization (trainable or fixed), and the trade-off between delay order and network size.

Experimental results show that the proposed delay mechanism achieves performance comparable to that of existing delay-based approaches while remaining computationally efficient. The proposed delay mechanism introduces either no additional

TABLE V: Test accuracy on the SHD dataset across combinations of number of neurons h and delay order n_d . All networks consist of two hidden layers with h neurons each, adLIF neuron model and $\mathbf{A}_{sd} \sim \text{Uniform}$ used as a fixed value in the \mathbf{A}_{sd} non-trainable case and as initialization in the \mathbf{A}_{sd} trainable case. Bold values indicate the best performance for each h value (per row).

| (a) \mathbf{A}_{sd} non-trainable. | | | | | |
|--------------------------------------|------------------------------------|------------------------------------|------------------|------------------------------------|--|
| h | No delay | $n_d = 10$ | $n_d = 50$ | $n_d = 100$ | |
| 512 | 92.5 \pm 0.7 % | 92.7 \pm 0.9 % | 90.8 \pm 1.5 % | 90.4 \pm 1.0 % | |
| 256 | 93.1 \pm 1.1 % | 92.1 \pm 0.5 % | 90.6 \pm 1.3 % | 89.9 \pm 0.6 % | |
| 128 | 92.0 \pm 0.4 % | 92.1 \pm 1.3 % | 89.8 \pm 1.2 % | 89.4 \pm 0.6 % | |
| 64 | 91.3 \pm 1.1 % | 91.8 \pm 1.3 % | 89.6 \pm 1.1 % | 89.4 \pm 1.8 % | |
| 32 | 88.7 \pm 2.2 % | 90.2 \pm 1.3 % | 86.8 \pm 1.4 % | 88.2 \pm 1.2 % | |
| 16 | 78.1 \pm 1.0 % | 86.9 \pm 1.2 % | 86.6 \pm 0.7 % | 87.1 \pm 1.2 % | |
| 8 | 60.1 \pm 7.4 % | 75.3 \pm 1.6 % | 77.3 \pm 2.2 % | 80.3 \pm 1.3 % | |

| (b) \mathbf{A}_{sd} trainable. | | | |
|----------------------------------|------------------------------------|------------------|------------------------------------|
| h | $n_d = 10$ | $n_d = 50$ | $n_d = 100$ |
| 512 | 92.7 \pm 0.9 % | 90.8 \pm 1.5 % | 90.4 \pm 1.0 % |
| 256 | 92.1 \pm 0.5 % | 90.6 \pm 1.3 % | 89.9 \pm 0.6 % |
| 128 | 92.1 \pm 1.3 % | 89.8 \pm 1.2 % | 89.4 \pm 0.6 % |
| 64 | 91.8 \pm 1.3 % | 89.6 \pm 1.1 % | 89.4 \pm 1.8 % |
| 32 | 90.2 \pm 1.3 % | 86.8 \pm 1.4 % | 88.2 \pm 1.2 % |
| 16 | 86.2 \pm 1.0 % | 84.1 \pm 1.2 % | 83.0 \pm 1.0 % |
| 8 | 72.6 \pm 2.5 % | 70.1 \pm 2.6 % | 73.8 \pm 1.9 % |

trainable parameters or only a small number relative to the total network size. Furthermore, we observe that incorporating delays significantly improves performance in smaller networks, where the delays can compensate for the restricted inherent capacity of the model due to the limited number of neurons.

IX. APPENDIX

A. Network and Training further details

Our code is based on the Sparch implementation [3]. During the training process, neuron parameters are clipped to remain within these boundaries as in [9] i.e. $\alpha \in [0.36, 0.96]$, $\beta \in [0.96, 0.99]$, $a \in [0, 1]$ and $b \in [0, 2]$.

We use hyperparameters based on previous works [9], [16], [48], in particular base $\text{LR} = 10^{-2}$, $\text{WD} = 10^{-5}$, dropout rate = 0.4, batch size = 128, and number of epochs = 50. No hyperparameter optimization has been performed.

B. Dataset further details

For the SHD dataset, similar to other works [16] [9] we used spatio-temporal bins to reduce the input dimensions. The input channels were reduced from 700 to 140 by binning every 5 consecutive channels.

The dataset was put in frames using the To-Frame [49] function with $\text{time-window} = 10000$, i.e. accumulation of events with time-windows of 10ms. The framed data set was used to load batches during both training and testing. During training, we use the data augmentation techniques `TimeNeurons_mask_aug` and `CutMix` following previous work [9] [16].

REFERENCES

- [1] W. Maass, “Networks of spiking neurons: The third generation of neural network models,” *Neural Networks*, vol. 10, no. 9, pp. 1659–1671, 1997.
- [2] M. Davies, A. Wild, G. Orchard, Y. Sandamirskaya, G. A. F. Guerra, P. Joshi, P. Plank, and S. R. Risbud, “Advancing neuromorphic computing with Loihi: A survey of results and outlook,” *Proceedings of the IEEE*, vol. 109, no. 5, pp. 911–934, 2021.
- [3] A. Bittar and P. N. Garner, “A surrogate gradient spiking baseline for speech command recognition,” *Frontiers in Neuroscience*, vol. 16, 2022.
- [4] S. F. Müller-Cleve, V. Fra, L. Khacef, A. Pequeño-Zurro, D. Klepatsch, E. Forno, D. G. Ivanovich, S. Rastogi, G. Urgese, F. Zenke, and C. Bartolozzi, “Braille letter reading: A benchmark for spatio-temporal pattern recognition on neuromorphic hardware,” *Frontiers in Neuroscience*, vol. 16 - 2022, 2022.
- [5] G. Gallego, T. Delbrück, G. Orchard, C. Bartolozzi, B. Taba, A. Censi, S. Leutenegger, A. J. Davison, J. Conradt, K. Daniilidis, and D. Scaramuzza, “Event-based vision: A survey,” *IEEE Transactions on Pattern Analysis and Machine Intelligence*, vol. 44, pp. 154–180, 2022.
- [6] C. E. Carr *et al.*, “Processing of temporal information in the brain,” *Annual review of neuroscience*, vol. 16, no. 1, pp. 223–243, 1993.
- [7] C. Carr and M. Konishi, “A circuit for detection of interaural time differences in the brain stem of the barn owl,” *Journal of Neuroscience*, vol. 10, no. 10, pp. 3227–3246, 1990.
- [8] W. Maass and M. Schmitt, “On the complexity of learning for spiking neurons with temporal coding,” *Information and Computation*, vol. 153, no. 1, pp. 26–46, 1999.
- [9] L. Deckers, L. Van Damme, W. Van Leeuwijk, I. J. Tsang, and S. Latré, “Co-learning synaptic delays, weights and adaptation in spiking neural networks,” *Frontiers in Neuroscience*, vol. 18, p. 1360300, 2024.
- [10] P. Sun, J. Achterberg, Z. Su, D. F. M. Goodman, and D. Akarca, “Exploiting heterogeneous delays for efficient computation in low-bit neural networks,” 2025. [Online]. Available: <https://arxiv.org/abs/2510.27434>
- [11] J. Göltz, J. Weber, L. Kriener, S. Billaudelle, P. Lake, J. Schemmel, M. Payvand, and M. A. Petrovici, “Delgrad: exact event-based gradients for training delays and weights on spiking neuromorphic hardware,” *Nature Communications*, vol. 16, 2025.
- [12] S. B. Shrestha and G. Orchard, “Slayer: Spike layer error reassignment in time,” *Advances in neural information processing systems*, vol. 31, 2018.
- [13] P. Sun, Y. Chua, P. Devos, and D. Botteldooren, “Learnable axonal delay in spiking neural networks improves spoken word recognition,” *Frontiers in Neuroscience*, vol. 17 - 2023, 2023.

[14] C. Diaz, G. Sanchez, G. Duchen, M. Nakano, and H. Perez, "An efficient hardware implementation of a novel unary spiking neural network multiplier with variable dendritic delays," *Neurocomputing*, vol. 189, pp. 130–134, 2016.

[15] E. Grappolini and A. Subramoney, "Beyond weights: Deep learning in spiking neural networks with pure synaptic-delay training," in *Proceedings of the 2023 International Conference on Neuromorphic Systems*, ser. ICONS '23. New York, NY, USA: Association for Computing Machinery, 2023.

[16] I. Hammouamri, I. Khalfaoui-Hassani, and T. Masquelier, "Learning delays in spiking neural networks using dilated convolutions with learnable spacings," *International Conference on Learning Representations (ICLR)*, 2024.

[17] M. Dominijanni, A. Ororbia, and K. W. Regan, "Extending spike-timing dependent plasticity to learning synaptic delays," 2025. [Online]. Available: <https://arxiv.org/abs/2506.14984>

[18] B. Mészáros, J. C. Knight, and T. Nowotny, "Learning delays through gradients and structure: emergence of spatiotemporal patterns in spiking neural networks," *Frontiers in Computational Neuroscience*, vol. 18, p. 1460309, 2024.

[19] K. G. Habashy, B. D. Evans, D. F. M. Goodman, and J. S. Bowers, "Adapting to time: Why nature may have evolved a diverse set of neurons," *PLOS Computational Biology*, vol. 20, no. 12, pp. 1–19, 12 2024.

[20] F. Moro, P. V. Aceituno, L. Kriener, and M. Payvand, "The role of temporal hierarchy in spiking neural networks," 2024.

[21] A. Queant, U. Rançon, B. R. Cottereau, and T. Masquelier, "Delrec: learning delays in recurrent spiking neural networks," 2025. [Online]. Available: <https://arxiv.org/abs/2509.24852>

[22] B. Mészáros, J. C. Knight, and T. Nowotny, "Efficient event-based delay learning in spiking neural networks," *arXiv preprint arXiv:2501.07331*, 2025.

[23] E. O. Neftci, H. Mostafa, and F. Zenke, "Surrogate gradient learning in spiking neural networks: Bringing the power of gradient-based optimization to spiking neural networks," *IEEE Signal Process. Magazine*, vol. 36, pp. 51–63, 2019.

[24] J.-P. Richard, "Time-delay systems: an overview of some recent advances and open problems," *Automatica*, vol. 39, no. 10, pp. 1667–1694, 2003.

[25] O. Sename, "Stability of time-delay systems, keqin gu, vladimir l. kharitonov, jie chen, birkhäuser, boston, 2003, isbn 0-8176-4212-9," *Automatica (Oxford)*, vol. 41, no. 12, pp. 2181–2183, 2005.

[26] A. Gu, K. Goel, and C. Ré, "Efficiently modeling long sequences with structured state spaces," 2022.

[27] A. Gupta, A. Gu, and J. Berant, "Diagonal state spaces are as effective as structured state spaces," in *Proceedings of the 36th International Conference on Neural Information Processing Systems*, 2022.

[28] D. Y. Fu, T. Dao, K. K. Saab, A. W. Thomas, A. Rudra, and C. Ré, "Hungry hungry hippos: Towards language modeling with state space models," *International Conference on Learning Representations (ICLR) 2023*, 2022.

[29] M. Zhang, K. K. Saab, M. Poli, T. Dao, K. Goel, and C. Ré, "Effectively modeling time series with simple discrete state spaces," *International Conference on Learning Representations (ICLR)*, 2023.

[30] P. Vincent-Lamarre, M. Calderini, and J.-P. Thivierge, "Learning long temporal sequences in spiking networks by multiplexing neural oscillations," *Frontiers in Computational Neuroscience*, vol. 14, 2020.

[31] M. Bal and A. Sengupta, "Rethinking spiking neural networks as state space models," 2024.

[32] S. Karilanova, S. Dey, and A. Özcelikkale, "State-space model inspired multiple-input multiple-output spiking neurons," in *2025 Neuro Inspired Computational Elements (NICE)*, 2025, pp. 1–9.

[33] S. Karilanova, S. Dey, and A. Özcelikkale, "Low-bit data processing using multiple-output spiking neurons with non-linear reset feedback," *IEEE Journal of Selected Topics in Signal Processing*, pp. 1–15, 2025.

[34] Y. Du, X. Liu, and Y. Chua, "Spiking structured state space model for monaural speech enhancement," in *IEEE Inter. Conf. on Acoustics, Speech and Signal Process. (ICASSP)*, 2024, pp. 766–770.

[35] S. Karilanova, M. Fabre, E. Neftci, and A. Özcelikkale, "Zero-shot temporal resolution domain adaptation for spiking neural networks," 2025. [Online]. Available: <https://arxiv.org/abs/2411.04760>

[36] L. Ljung, *System Identification: Theory for the user*. Prentice Hall PTR, 1987.

[37] S. Ioffe and C. Szegedy, "Batch normalization: accelerating deep network training by reducing internal covariate shift," in *Proceeding. of the International Conference on Machine Learning (ICML)*, vol. 37, 2015, p. 448–456.

[38] I. Loshchilov and F. Hutter, "Decoupled weight decay regularization," in *International Conference on Learning Representations (ICLR)*, 2019.

[39] B. Cramer, Y. Stradmann, J. Schemmel, and F. Zenke, "The heidelberg spiking data sets for the systematic evaluation of spiking neural networks," *IEEE Trans. on Neural Networks and Learning Systems*, vol. 33, no. 7, pp. 2744–2757, 2022.

[40] G. Boesherz, G. Indiveri, M. Nair, and A. Renner, "Accurate mapping of RNNs on neuromorphic hardware with adaptive spiking neurons," *International Conference on Neuromorphic Systems (ICONS)*, pp. 376–380, 2024.

[41] A. Patiño-Saucedo, A. Yousefzadeh, G. Tang, F. Corradi, B. Linares-Barranco, and M. Sifalakis, "Empirical study on the efficiency of spiking neural networks with axonal delays, and algorithm-hardware benchmarking," in *2023 IEEE International Symposium on Circuits and Systems (ISCAS)*, 2023, pp. 1–5.

[42] R. Meijer, P. Detterer, A. Yousefzadeh, A. Patiño-Saucedo, G. Tang, K. Vadivel, Y. Xu, M.-D. Gomony, F. Corradi, B. Linares-Barranco, and M. Sifalakis, "Efficient synaptic delay implementation in digital event-driven ai accelerators," 2025.

[43] S. D'Agostino, F. Moro, T. Torchetti, Y. Demirag, L. Grenouillet, N. Castellani, G. Indiveri, E. Vianello, and M. Payvand, "Denram: neuromorphic dendritic architecture with rram for efficient temporal processing with delays," *Nature Communications*, vol. 15, 2024.

[44] M. Davies, N. Srinivasa, T.-H. Lin, G. Chinya, Y. Cao, S. H. Choday, G. Dimou, P. Joshi, N. Imam, S. Jain, Y. Liao, C.-K. Lin, A. Lines, R. Liu, D. Mathaiikutty, S. McCoy, A. Paul, J. Tse, G. Venkataraman, Y.-H. Weng, A. Wild, Y. Yang, and H. Wang, "Loihi: A neuromorphic manycore processor with on-chip learning," *IEEE Micro*, vol. 38, no. 1, pp. 82–99, 2018.

[45] F. Akopyan, J. Sawada, A. Cassidy, R. Alvarez-Icaza, J. Arthur, P. Merolla, N. Imam, Y. Nakamura, P. Datta, G.-J. Nam, B. Taba, M. Beakes, B. Brezzo, J. B. Kuang, R. Manohar, W. P. Risk, B. Jackson, and D. S. Modha, "Truenorth: Design and tool flow of a 65 mw 1 million neuron programmable neurosynaptic chip," *IEEE Transactions on Computer-Aided Design of Integrated Circuits and Systems*, vol. 34, no. 10, pp. 1537–1557, 2015.

[46] S. B. Furber, F. Galluppi, S. Temple, and L. A. Plana, "The spinnaker project," *Proceedings of the IEEE*, vol. 102, no. 5, pp. 652–665, 2014.

[47] A. Yousefzadeh, G.-J. van Schaik, M. Tahaghghi, P. Detterer, S. Traffero, M. Hijdra, J. Stuijt, F. Corradi, M. Sifalakis, and M. Konijnenburg, "Seneca: Scalable energy-efficient neuromorphic computer architecture," in *2022 IEEE 4th International Conference on Artificial Intelligence Circuits and Systems (AICAS)*, 2022, pp. 371–374.

[48] M. Schöne, N. M. Sushma, J. Zhuge, C. Mayr, A. Subramoney, and D. Kappel, "Scalable event-by-event processing of neuromorphic sensory signals with deep state-space models," *IEEE/ACM International Conference on Neuromorphic Systems (ICONS)*, 2024.

[49] G. Lenz, K. Chaney, S. B. Shrestha, O. Oubari, S. Picaud, and G. Zarrella, "Tonic: event-based datasets and transformations." 2021, <https://tonic.readthedocs.io>.